

General Relativity Tests with Pulsars

I. H. Stairs

*Dept. of Physics and Astronomy, University of British Columbia, 6224 Agricultural Road, Vancouver, BC V6T 1Z1
Canada*

Tests of general relativity from equivalence principle violations to binary orbital effects in the strong-gravitational-field regime can be achieved using observations of radio pulsars. This article provides an overview of the process, including recent updates of classic tests and new experiments made possible by the recently discovered double-pulsar system.

1. INTRODUCTION

The potential of pulsars for high-precision tests of the predictions of general relativity (GR) was recognized immediately upon the discovery of the first pulsar binary system, PSR B1913+16 [1–5]. Since then, pulsars have provided stringent tests of equivalence principle violations and both radiative and quasi-static strong-field effects. This article presents an overview of these tests (see also [6] for a fuller though now somewhat dated description of much of this material, and [7] for an intermediate version), including the exciting recent discovery of a double-pulsar system [8, 9].

2. OVERVIEW OF PULSAR OBSERVATIONS

Radio pulsars were discovered in 1967 [10], and quickly identified with rotating neutron stars [11, 12]. The lighthouse-like beams of radio waves emitted from a pulsar’s magnetic poles may hit the Earth once per rotation of the neutron star, producing a “pulse” of emission detectable by powerful radio telescopes. Pulsar timing takes advantage of the tremendous overall stability of pulsar rotation to measure tiny deviations from perfect observed regularity, and hence to derive science concerning neutron stars themselves, evolution of stellar systems, our Galaxy, and even cosmology.

While most of the roughly 1700 currently known pulsars have spin periods close to 1 second and estimated dipolar magnetic fields within a couple of orders of magnitude of 10^{12} G, there is an important separate class of older “millisecond” or “recycled” pulsars [13] which have been spun up to faster periods by accretion of matter and angular momentum from an evolving companion star (see, e.g., [14] and [15] for reviews of the evolution of such binary systems). It is precisely these recycled pulsars that form the most valuable resource for tests of GR.

Despite nearly 40 years of effort, there is still little consensus on the pulsar radio emission mechanism. Fortunately, although individual pulses display enormous variations in shape and intensity, a profile “integrated” over several hundred or thousand pulses (i.e., a few minutes) yields a shape – a “standard profile” – that is reproducible for a given pulsar at a given frequency. This allows us to use the integrated pulse shape as a tool for precision timing purposes without needing to understand the detailed physics behind its production.

Pulsar observations are usually conducted at radio frequencies from a few hundred MHz to a few GHz. At the lowest frequencies, pulsar signals are comparatively strong (e.g., [16]), but propagation effects (scattering, scintillation and dispersion) in the interstellar medium can significantly distort the received pulse shape. The effects of scattering can be reduced by observing at higher frequencies, and the effects of scintillation by using wide instrumental bandwidths. Dispersive smearing can be mitigated either by using a filterbank instrument, in which the observing bandpass is divided into many small channels before the signal is detected, or, preferably, by coherent dedispersion [17], in which the full amplitude and phase information of the signal are obtained, and the inverse of the frequency-dependent dispersive filter is applied in hardware or software (e.g., [18–20]). This technique provides the closest reproduction of the pulsed signal as emitted by the pulsar and hence the best basis from which to derive timing information; many of the results discussed below rely on such instrumentation.

Once dispersion has been removed, the resultant time series is typically integrated or “folded” modulo the pulse period predicted for the observatory’s reference frame. The pulse period may not be very easily predicted from the discovery period, especially if the pulsar happens to be in a binary system. The goal of pulsar timing is to develop a model of the pulse phase as a function of time, so that all future pulse arrival times can be predicted with a good degree of accuracy.

The profile accumulated over several minutes is compared by cross-correlation with the standard profile for the pulsar at that observing frequency. A commonly used version of the cross-correlation algorithm compares the two profiles in the frequency domain [21], although this approach can lead to some systematics depending on the observations used to produce the standard profile [22]. Once the phase shift of the observed profile relative to the standard profile is known, that offset is added to the start time of the observation in order to yield a “Time of Arrival” (TOA) that is representative of that few-minute integration. In practice, observers frequently use a time- and phase-stamp near the middle of the integration in order to minimize systematic errors due to a poorly known pulse period. As a rule, pulse timing precision is best for bright pulsars with short spin periods, narrow profiles with steep edges, and little if any profile corruption due to interstellar scattering.

Once TOAs are obtained, it becomes possible to fit a model of the pulsar’s timing behavior, enumerating every rotation of the neutron star. Based on the magnetic dipole model [11, 12], the pulsar is expected to lose rotational energy and thus “spin down”. The primary component of the timing model is therefore a Taylor expansion of the pulse phase ϕ with time t :

$$\phi = \phi_0 + \nu(t - t_0) + \frac{1}{2}\dot{\nu}(t - t_0)^2 + \dots \quad (1)$$

where ϕ_0 and t_0 are a reference phase and time, respectively, and the pulse frequency ν is the time derivative of the pulse phase. Note that the fitted parameters ν and $\dot{\nu}$ and the magnetic dipole model can be used to derive an estimate of the surface magnetic field $B \sin \alpha$:

$$B \sin \alpha = \left(\frac{-3I\dot{\nu}c^3}{8\pi^2 R^6 \nu^3} \right)^{1/2} \approx 3.2 \times 10^{19} \left(\frac{-\dot{\nu}}{\nu^3} \right)^{1/2} G, \quad (2)$$

where α is the inclination angle between the pulsar spin axis and the magnetic dipole axis, R is the radius of the neutron star, about 10^6 cm, and the moment of inertia is $I \simeq 10^{45}$ g cm². In turn, integration of the energy loss, along with the assumption that the pulsar was born with infinite spin frequency, yields a “characteristic age” τ_c for the pulsar:

$$\tau_c = -\frac{\nu}{2\dot{\nu}}. \quad (3)$$

Equation 1 refers to pulse frequencies and times in a reference frame that is inertial relative to the pulsar, and can be used only once TOAs derived in the rest frame of a telescope on the Earth have been translated to such a reference frame. The best approximation available for an inertial reference frame is that of the Solar System Barycenter (SSB), and the TOA conversion is typically uses the “DE200” or “DE405” ephemerides from the Jet Propulsion Laboratory [23, 24]. Some of the tests of GR described below still require correcting for the small relative accelerations of the SSB and the center-of-mass frames of binary pulsar systems. The required transformation between a TOA at the telescope, τ , and the emission time t from the pulsar is:

$$t = \tau - D/f^2 + \Delta_{R\odot} + \Delta_{E\odot} - \Delta_{S\odot} - \Delta_R - \Delta_E - \Delta_S. \quad (4)$$

Here D/f^2 accounts for the dispersive delay in seconds of the observed pulse at radio frequency f relative to infinite frequency. The Roemer term, $\Delta_{R\odot}$, takes out the travel time across the Solar System based on the relative positions of the pulsar and the telescope, including, if needed, the proper motion and parallax of the pulsar. The Einstein delay, $\Delta_{E\odot}$, accounts for the time dilation and gravitational redshift due to the Sun and other masses in the Solar System, while the Shapiro delay, $\Delta_{S\odot}$, expresses the excess delay to the pulsar signal as it travels through the gravitational well of the Sun — a maximum delay of about $120 \mu\text{s}$ at the limb of the Sun. See [25] for a fuller discussion of these terms.

The terms Δ_R , Δ_E , Δ_S in Equation 4 describe the equivalent ‘‘Roemer’’, ‘‘Einstein’’ and ‘‘Shapiro’’ delays within a pulsar binary system. The majority of binary pulsar orbits are adequately described by five Keplerian parameters: the orbital period P_b , the projected semi-major axis x , the eccentricity e , and the longitude ω and epoch T_0 of periastron. The angle ω is measured from the line of nodes, Ω , where the pulsar orbit intersects the plane of the sky and the pulsar is moving away from the SSB. In many cases, one or more relativistic corrections to the Keplerian parameters must also be fit. The best modern timing model [26–29] incorporates a number of ‘‘post-Keplerian’’ timing parameters which are included in the description of the three delay terms. These are fit in a completely phenomenological manner and hence do not assume that any particular theory of gravity describes the pulsar orbit. The delays are written primarily in terms of the phase of the orbit, defined by the eccentric anomaly u and true anomaly $A_e(u)$, as well as ω , P_b and their time derivatives, if needed. These are related by:

$$u - e \sin u = 2\pi \left[\left(\frac{T - T_0}{P_b} \right) - \frac{\dot{P}_b}{2} \left(\frac{T - T_0}{P_b} \right)^2 \right], \quad (5)$$

$$A_e(u) = 2 \arctan \left[\left(\frac{1+e}{1-e} \right)^{1/2} \tan \frac{u}{2} \right], \quad (6)$$

$$\omega = \omega_0 + \left(\frac{P_b \dot{\omega}}{2\pi} \right) A_e(u), \quad (7)$$

where ω_0 is the reference value of ω at time T_0 . The delay terms then become:

$$\Delta_R = x \sin \omega (\cos u - e(1 + \delta_r)) + x(1 - e^2(1 + \delta_\theta)^2)^{1/2} \cos \omega \sin u, \quad (8)$$

$$\Delta_E = \gamma \sin u, \quad (9)$$

$$\Delta_S = -2r \ln \left\{ 1 - e \cos u - s \left[\sin \omega (\cos u - e) + (1 - e^2)^{1/2} \cos \omega \sin u \right] \right\}. \quad (10)$$

Here γ represents the time dilation and gravitational redshift due to the pulsar’s motion in the gravitational potential of its companion, and r and s give the ‘‘range’’ and ‘‘shape’’ of the Shapiro delay. Together with the orbital period derivative \dot{P}_b and the advance of periastron $\dot{\omega}$, they make up the post-Keplerian timing parameters that can be fit for various pulsar binaries. A fuller description of the timing model also includes the aberration parameters δ_r and δ_θ , but these parameters are usually indistinguishable from the other orbital parameters. The interpretation of the measured post-Keplerian timing parameters will be discussed in the context of double-neutron-star tests of GR in Section 4.

A pulsar timing model can therefore require a large number of parameters. Most observers accomplish the model fitting, accounting for all the delay terms, using the program TEMPO ¹. Accurate time-keeping is naturally of primary importance in pulsar modeling. General practice is to derive the time-stamp on each observation from the Observatory’s local time standard — typically a Hydrogen maser — and to apply, retroactively, corrections to well-maintained time standards such as UTC(BIPM), Universal Coordinated Time as maintained by the Bureau International des Poids et Mesures.

3. EQUIVALENCE PRINCIPLE VIOLATIONS

Equivalence principles describe our expectations of experimental outcomes in different reference frames; for full descriptions see, for example, [30] or [31]. The Weak Equivalence Principle (WEP), formalized by Newton, states that

¹<http://pulsar.princeton.edu/tempo>

in an external gravitational field, objects of different compositions and masses will experience the same acceleration. The Einstein Equivalence Principle (EEP) extends this idea to include Lorentz invariance (non-existence of preferred reference frames) and positional invariance (non-existence of preferred locations) for non-gravitational experiments, predicting that these experiments will have the same outcomes in all inertial reference frames. The Strong Equivalence Principle (SEP) adds Lorentz and positional invariance for gravitational experiments, thus including experiments on objects with strong self-gravitation. GR incorporates the SEP, but alternate theories of gravity may violate all or parts of it.

The parametrized post-Newtonian (PPN) formalism [32] provides a uniform description of the weak-gravitational-field limit and facilitates comparisons of different gravitational theories in this limit. This formalism has 10 parameters ($\gamma_{\text{PPN}}, \beta, \xi, \alpha_1, \alpha_2, \alpha_3, \zeta_1, \zeta_2, \zeta_3$ and ζ_4); see [33] for full descriptions and physical meanings of these parameters. This formalism has been extended [34, 35] to include strong-field effects for generalized tensor-multiscalar gravitational theories. This allows a better understanding of limits in the strong-field regime imposed by systems including pulsars and white dwarfs, for which the amounts of self-gravitation are very different. Here, for instance, α_1 becomes $\hat{\alpha}_1 = \alpha_1 + \alpha'_1(c_1 + c_2) + \dots$, where c_i describes the ‘‘compactness’’ of mass m_i . The compactness can be written $c_i = -2\partial \ln m_i / \partial \ln G \simeq -2(E_i^{\text{grav}} / (mc^2))_i$, where G is Newton’s constant and E_i^{grav} is the gravitational self-energy of mass m_i . The compactness is about -0.2 for a neutron star (NS) and -10^{-4} for a white dwarf (WD). Pulsar timing sets limits on $\hat{\alpha}_1$, which tests for the existence of preferred-frame effects (violations of Lorentz invariance) and $\hat{\alpha}_3$, which, in addition to testing for preferred-frame effects, also implies non-conservation of momentum if non-zero. (A test of $\hat{\zeta}_2$, which is also a non-conservative parameter, relies on the second period derivative of the double-neutron-star binary PSR B1913+16 [36]. As a measurement of this quantity could also be due to timing noise or to geodetic precession [37] this test will not be considered further.) Pulsars can also be used to set limits on other SEP-violation effects which constrain combinations of the PPN parameters: the Nordtvedt (‘‘gravitational Stark’’) effect, dipolar gravitational radiation, and variation of Newton’s constant.

3.1. Strong Equivalence Principle

Direct tests of the SEP through Lunar Laser Ranging (LLR) experiments were first suggested by [38]. As the masses of Earth and the Moon contain different fractional contributions from self-gravitation, a violation of the SEP would cause them to fall differently in the Sun’s gravitational field and ‘‘polarize’’ the orbit in the direction of the Sun. LLR tests have set a limit of $|\eta| < 0.001$ (e.g., [33, 39]), where η is a combination of PPN parameters:

$$\eta = 4\beta - \gamma - 3 - \frac{10}{3}\xi - \alpha_1 + \frac{2}{3}\alpha_2 - \frac{2}{3}\zeta_1 - \frac{1}{3}\zeta_2. \quad (11)$$

The strong-field formalism uses the parameter Δ_i [40], which for object ‘‘ i ’’ may be written as:

$$\begin{aligned} \left(\frac{m_{\text{grav}}}{m_{\text{inertial}}} \right)_i &= 1 + \Delta_i \\ &= 1 + \eta \left(\frac{E^{\text{grav}}}{mc^2} \right)_i + \eta' \left(\frac{E^{\text{grav}}}{mc^2} \right)_i^2 + \dots \end{aligned} \quad (12)$$

Pulsar–white dwarf systems constrain the difference $\Delta_{\text{net}} = \Delta_{\text{pulsar}} - \Delta_{\text{companion}}$ [40]. If the SEP is violated, the equations of motion for such a system will contain an extra acceleration $\Delta_{\text{net}}\mathbf{g}$, where \mathbf{g} is the gravitational acceleration due to the Galaxy. This term will influence the evolution of the orbit of the system. For low-eccentricity orbits, the largest effect will be to force the eccentricity toward alignment with the projection of \mathbf{g} onto the orbital plane of the system. Therefore the time evolution of the eccentricity vector will not only depend on the usual GR-predicted relativistic advance of periastron ($\dot{\omega}$) but will also include a constant term. The time-dependent eccentricity vector may be written as [40]:

$$\mathbf{e}(t) = \mathbf{e}_F + \mathbf{e}_R(t), \quad (13)$$

where $\mathbf{e}_R(t)$ is the $\dot{\omega}$ -induced rotating eccentricity vector, and \mathbf{e}_F is the forced component. In terms of Δ_{net} , the magnitude of \mathbf{e}_F is [40, 41]:

$$|\mathbf{e}_F| = \frac{3}{2} \frac{\Delta_{\text{net}} \mathbf{g}_\perp}{\dot{\omega} a (2\pi/P_b)}, \quad (14)$$

where \mathbf{g}_\perp is the projection of the gravitational field onto the orbital plane, and $a = x/(\sin i)$ is the semi-major axis of the orbit. For small-eccentricity systems, this reduces to:

$$|\mathbf{e}_F| = \frac{1}{2} \frac{\Delta_{\text{net}} \mathbf{g}_\perp c^2}{FGM(2\pi/P_b)^2}, \quad (15)$$

where M is the total mass of the system, and, in GR, $F = 1$ and G is Newton's constant. Here \mathbf{g}_\perp is the projection of the Galactic acceleration vector onto the plane of the orbit, and is given by [40]:

$$|\mathbf{g}_\perp| = |\mathbf{g}| [1 - (\cos i \cos \lambda + \sin i \sin \lambda \sin(\phi - \Omega))^2]^{1/2}, \quad (16)$$

where ϕ is the position angle of the projection of the gravitational acceleration vector \mathbf{g} onto the plane of the sky, and λ is the angle between the line from pulsar to Earth and \mathbf{g} . Deriving \mathbf{e}_F requires knowledge of the Galactic acceleration at the pulsar position; this can be obtained from potential models of the Galaxy (e.g., [42]).

Pulsars with large values of P_b^2/e are clearly prime candidates to test for non-zero Δ_{net} . However, two age-related restrictions are also needed [40, 41]. First of all, the pulsar must be sufficiently old that the $\dot{\omega}$ -induced rotation of \mathbf{e} has completed many turns and $\mathbf{e}_R(t)$ can be assumed to be randomly oriented. This requires that the characteristic age $\tau_c \gg 2\pi/\dot{\omega}$ and thus young pulsars cannot be used. Secondly, $\dot{\omega}$ itself must be larger than the rate of Galactic rotation, so that the projection of \mathbf{g} onto the orbit can be assumed to be constant. According to [41], this holds true for pulsars with orbital periods of less than about 1000 days.

Converting equation 15 to a limit on Δ_{net} requires some statistical arguments to deal with the unknowns in the problem. Usually, the orbital inclination angle i , the masses m_1 and m_2 , the angle of the Line of Nodes Ω and the pulsar distance are not very well constrained, although there are some notable exceptions [43, 44]. The most vexing problem has historically been the issue of how to treat the unknown angle between \mathbf{e}_F and the “natural” eccentricity \mathbf{e}_R . Limits based on “worst-case” cancellation scenarios have been obtained for individual pulsars [40] and an ensemble of pulsars [41, 45], with [45] attempting to account for selection effects by using a larger set of pulsars, even those with low values of P_b^2/e . Recently, a new limit has been obtained, again using the full set of pulsars that likely have similar evolutionary histories, but using a Bayesian analysis to calculate probability density functions (pdfs) for each pulsar, making simple assumptions about the prior distributions of \mathbf{e}_R and the angle it makes to \mathbf{e}_F , and using whatever geometrical information is available for each pulsar, including, for the first time, the observed longitude of periastron. This results in a 95% confidence upper limit on $|\Delta|$ of 5.6×10^{-3} [46]. Prospects for improving the limits come from the discovery of new suitable pulsars, and from better-measured or constrained values of eccentricity and longitude of periastron from long-term timing of the current set of pulsars.

3.2. Preferred-Frame Effects and Non-conservation of Momentum

3.2.1. Limits on $\hat{\alpha}_1$

A non-zero $\hat{\alpha}_1$ implies that the velocity \mathbf{w} of a binary pulsar system (relative to a “universal” background reference frame given by the Cosmic Microwave Background, or CMB) will affect its orbital evolution. In a manner similar to the effects of a non-zero Δ_{net} , the time evolution of the eccentricity will depend on both $\dot{\omega}$ and a term which tries to force the semi-major axis of the orbit to align with the projection of the system velocity onto the orbital plane.

The analysis proceeds in a similar fashion to that for Δ_{net} , except that the magnitude of \mathbf{e}_F is now written as [47, 48]:

$$|\mathbf{e}_F| = \frac{1}{12} \hat{\alpha}_1 \left| \frac{m_1 - m_2}{m_1 + m_2} \right| \frac{|w_\perp|}{[G(m_1 + m_2)(2\pi/P_b)]^{1/3}}, \quad (17)$$

where w_{\perp} is the projection of the system velocity onto the orbital plane. The angle λ , used in determining this projection in a manner similar to that of equation 16, is now the angle between the line of sight to the pulsar and the absolute velocity of the binary system.

The figure of merit for systems used to test $\hat{\alpha}_1$ is $P_b^{1/3}/e$. As for the Δ_{net} test, the systems must be old, so that $\tau_c \gg 2\pi/\dot{\omega}$, and $\dot{\omega}$ must be larger than the rate of Galactic rotation. Examples of suitable systems are PSR J2317+1439 [48, 49] with a last published value of $e < 1.2 \times 10^{-6}$ in 1996 [50], and PSR J1012+5307, with $e < 8 \times 10^{-7}$ [51]. This latter system is especially valuable because observations of its white-dwarf component yield a radial velocity measurement [52], eliminating the need to find a lower limit on an unknown quantity. The most recent limit is $\hat{\alpha}_1 < 1.4 \times 10^{-4}$ [45]. This is comparable in magnitude to the weak-field results from lunar laser ranging, but incorporates strong field effects as well. In principle, this test should also be updated using the Bayesian method, but the pulsars with good figures of merit tend to be those with very short orbital periods and possibly different evolutionary histories, so it is much more difficult to be assured of using a set of pulsars that is truly representative of the relevant population.

3.2.2. Limits on $\hat{\alpha}_3$

Tests of $\hat{\alpha}_3$ can be derived from both binary and single pulsars, using somewhat different techniques. A non-zero $\hat{\alpha}_3$, which implies both a violation of local Lorentz invariance and non-conservation of momentum, will cause a rotating body to experience a self-acceleration \mathbf{a}_{self} in a direction orthogonal to both its spin $\boldsymbol{\Omega}_S$ and its absolute velocity \mathbf{w} [53]:

$$\mathbf{a}_{\text{self}} = -\frac{1}{3}\hat{\alpha}_3 \frac{E^{\text{grav}}}{(m c^2)} \mathbf{w} \times \boldsymbol{\Omega}_S. \quad (18)$$

Thus the self-acceleration depends strongly on the compactness of the object.

An ensemble of single (isolated) pulsars can be used to set a limit on $\hat{\alpha}_3$ in the following manner. For any given pulsar, it is likely that some fraction of the self-acceleration will be directed along the line of sight to the Earth. Such an acceleration will contribute to the observed period derivative \dot{P} via the Doppler effect, by an amount:

$$\dot{P}_{\hat{\alpha}_3} = \frac{P}{c} \hat{\mathbf{n}} \cdot \mathbf{a}_{\text{self}}, \quad (19)$$

where $\hat{\mathbf{n}}$ is a unit vector in the direction from the pulsar to the Earth. One analysis [31] assumes random orientations of both the pulsar spin axes and velocities, and finds that, on average, $|\dot{P}_{\hat{\alpha}_3}| \simeq 5 \times 10^{-5} |\hat{\alpha}_3|$, independent of the pulse period. The *sign* of the $\hat{\alpha}_3$ contribution to \dot{P} , however, may be positive or negative for any individual pulsar, thus if there were a large contribution on average, one would expect to observe pulsars with both positive and negative total period derivatives. Young pulsars in the field of the Galaxy (pulsars in globular clusters suffer from unknown accelerations from the cluster gravitational potential and do not count toward this analysis) all show positive period derivatives, typically around 10^{-14} s/s. Thus the maximum possible contribution from $\hat{\alpha}_3$ must also be considered to be of this size, and the limit is given by $|\hat{\alpha}_3| < 2 \times 10^{-10}$ [31].

This test can also be applied to a set of millisecond pulsars [54]; these have much smaller period derivatives, on the order of 10^{-20} s/s. Here it is also necessary to account for the ‘‘Shklovskii effect’’ [55] in which a similar Doppler-shift addition to the period derivative results from the transverse motion of the pulsar on the sky:

$$\dot{P}_{\text{pm}} = P \mu^2 \frac{d}{c} \quad (20)$$

where μ is the proper motion of the pulsar and d is the distance between the Earth and the pulsar. The distance is usually poorly determined, with uncertainties of typically 30% resulting from models of the dispersive free electron density in the Galaxy [56, 57]. Nevertheless, once this correction (which is always positive) is applied to the observed period derivatives for isolated millisecond pulsars, a limit on $|\hat{\alpha}_3|$ on the order of 10^{-15} results [54, 58].

In the case of a binary pulsar–white-dwarf system, both bodies experience a self-acceleration. The most important effect is a coupling of the spins to the absolute motion of the center of mass [58]. Both the compactness and the

spin of the pulsar will completely dominate those of the white dwarf, making the net acceleration of the two bodies effectively:

$$\mathbf{a}_{\text{self}} = \frac{1}{6} \hat{\alpha}_3 c_p \mathbf{w} \times \boldsymbol{\Omega}_{\text{Sp}}, \quad (21)$$

where c_p and $\boldsymbol{\Omega}_{\text{Sp}}$ denote the compactness and spin angular frequency of the pulsar, respectively, and \mathbf{w} is the velocity of the system. For evolutionary reasons (e.g., [15]), the spin axis of the pulsar may be assumed to be aligned with the orbital angular momentum of the system, hence the net effect of the acceleration will be to induce a polarization of the eccentricity vector within the orbital plane. The forced eccentricity term may be written as:

$$|\mathbf{e}_F| = \hat{\alpha}_3 \frac{c_p |\mathbf{w}|}{24\pi} \frac{P_b^2}{P} \frac{c^2}{G(m_1 + m_2)} \sin \beta \quad (22)$$

where β is the (unknown) angle between \mathbf{w} and $\boldsymbol{\Omega}_{\text{Sp}}$, and P is, as usual, the spin period of the pulsar: $P = 2\pi/\Omega_{\text{Sp}}$.

The figure of merit for systems used to test $|\hat{\alpha}_3|$ is $P_b^2/(eP)$. The additional requirements of $\tau_c \gg 2\pi/\dot{\omega}$ and $\dot{\omega}$ being larger than the rate of Galactic rotation also hold, so the same pulsars should be used in the Bayesian analysis as for $|\Delta_{\text{net}}|$. The 95% confidence limit derived in this manner is $|\hat{\alpha}_3| < 4 \times 10^{-20}$ [46].

3.3. Strong Equivalence Principle: Dipolar Gravitational Radiation

General Relativity predicts gravitational radiation from the time-varying mass quadrupole of a binary pulsar system. The spectacular confirmation of this prediction will be discussed in section 4 below. GR does not, however, predict *dipolar* gravitational radiation, though many theories that violate the SEP do. In these theories, dipolar gravitational radiation results from the difference in gravitational binding energy of the two components of a binary. For this reason, neutron star–white dwarf binaries are the ideal laboratories to test the strength of such dipolar emission. The expected rate of change of the period of a circular orbit due to dipolar emission can be written as [31, 59]:

$$\dot{P}_{\text{b Dipole}} = -\frac{4\pi^2 G_*}{c^3 P_b} \frac{m_1 m_2}{m_1 + m_2} (\alpha_{c_1} - \alpha_{c_2})^2, \quad (23)$$

where $G_* = G$ in GR, and α_{c_i} is the coupling strength of body “ i ” to a scalar gravitational field [59]. (Similar expressions can be derived when casting $\dot{P}_{\text{b Dipole}}$ in terms of the parameters of specific tensor-scalar theories, such as Brans-Dicke theory [60]. Equation 23, however, tests a more general class of theories.) The best test systems here are pulsar–white dwarf binaries with short orbital periods, where $\alpha_{c_1} \gg \alpha_{c_2}$ so that a strong limit can be set on the coupling of the pulsar itself. The best test in a recycled-pulsar system comes from PSR J0751+1807, which sets a 95% confidence limit of $(\alpha_{c_1} - \alpha_{c_2})^2 < 7 \times 10^{-5}$ [61]. It should be noted that this limit depends on the unknown equation of state of the neutron stars.

The young-pulsar–white-dwarf system PSR J1141–6545 [62] is eccentric and therefore expected to emit large amounts of quadrupolar gravitational radiation. The resulting orbital period derivative has recently been measured [63, 64] and found to be in good agreement with the predictions of GR, thus this system can also be used to exclude dipolar radiation [65] and to set very strong limits on tensor-scalar theories [66].

Limits may also be derived from double-neutron-star systems (e.g., [67, 68]), although here the difference in the coupling constants is small and so the expected amount of dipolar radiation is also small compared to the quadrupole emission. However, certain alternative gravitational theories in which the quadrupolar radiation predicts a *positive* orbital period derivative independently of the strength of the dipolar term (e.g., [69–71]) are ruled out by the observed decreasing orbital period in these systems [72].

3.4. Preferred-location Effects: Variation of Newton’s Constant

Theories that violate the SEP by allowing for preferred locations (in time as well as space) may permit Newton’s constant, G , to vary. In general, variations in G are expected to occur on the timescale of the age of the Universe,

such that $\dot{G}/G \sim H_0 \sim 0.7 \times 10^{-10} \text{ yr}^{-1}$, where H_0 is the Hubble constant. Three different pulsar-derived tests can be applied to these predictions, as a SEP-violating time-variable G would be expected to alter the properties of neutron stars and white dwarfs, and to affect binary orbits.

By affecting the gravitational binding of neutron stars, a non-zero \dot{G} would reasonably be expected to alter the moment of inertia of the star and hence change its spin on the same timescale [73]. This can be written [74]:

$$\left(\frac{\dot{P}}{P}\right)_{\dot{G}} = \left(\frac{\partial \ln I}{\partial \ln G}\right)_N \frac{\dot{G}}{G}, \quad (24)$$

where I is the moment of inertia of the neutron star, about 10^{45} g cm^2 , and N is the (conserved) total number of baryons in the star. If this represents the *only* contribution to the observed \dot{P} of PSR B0655+64, in a manner reminiscent of the test of $\hat{\alpha}_3$ described above, the upper limit is $|\dot{G}/G| \leq (2.2 - 5.5) \times 10^{-11} \text{ yr}^{-1}$, depending on the stiffness of the neutron star equation of state [74]. Similar reasoning can be applied to PSR J2019+2425 [75] which has a characteristic age of 27 Gyr once the ‘‘Shklovskii’’ correction is applied [76]. Again depending on the equation of state, the upper limits from this pulsar are $|\dot{G}/G| \leq (1.4 - 3.2) \times 10^{-11} \text{ yr}^{-1}$ [77]. These values are similar to those obtained by solar-system experiments such as radar ranging to the Viking Lander on Mars (e.g., [78, 79]). Several other millisecond pulsars, once ‘‘Shklovskii’’ and Galactic-acceleration corrections are taken into account, have similarly large characteristic ages (e.g. [50, 80]).

In a binary system, a varying G will affect the individual stars and the total mass and angular momentum of the binary system, causing an orbital period derivative that may be written as [81, 82]:

$$\left(\frac{\dot{P}_b}{P_b}\right)_{\dot{G}} = - \left[2 - \left(\frac{m_1 c_1 + m_2 c_2}{m_1 + m_2}\right) - \frac{3}{2} \left(\frac{m_1 c_2 + m_2 c_1}{m_1 + m_2}\right) \right] \frac{\dot{G}}{G}. \quad (25)$$

The best limits again come from neutron-star–white-dwarf systems. In particular, PSR J1713+0747 yields an upper limit of $|\dot{P}_b/P_b|_{\dot{G}} \leq 3.2 \times 10^{-12} \text{ yr}^{-1}$ [44, 61], far more stringent than any other pulsar test and comparable to the best \dot{G}/G tests available from lunar laser ranging [83].

3.4.1. Changes in the Chandrasekhar Mass

The Chandrasekhar mass, M_{CH} , is the maximum mass possible for a white dwarf supported against gravitational collapse by electron degeneracy pressure [84]. Its value — about $1.4 M_{\odot}$ — depends on Newton’s constant: $M_{\text{CH}} \sim (\hbar c/G)^{3/2}/m_{\text{N}}^2$, where \hbar is Planck’s constant and m_{N} is the neutron mass. Under the assumption that M_{CH} sets the typical neutron star mass, one may check for any changes in the average neutron star mass over the lifetime of the Universe. The ages of double-neutron-star systems range from less than 1 Gyr for systems in the field of the Galaxy to 12 or 13 Gyr for those in globular clusters. A Bayesian analysis of the systems known in 1996 provides a limit of $\dot{G}/G = (-0.6 \pm 4.2) \times 10^{-12} \text{ yr}^{-1}$ at the 95% confidence level [85]. With the recent profusion of new double-neutron-star binaries and several globular-cluster binaries that may soon yield precise mass measurements (e.g., [86]), an update of this test should prove interesting in the near future.

4. TESTS OF GR — STRONG-FIELD GRAVITY

The best-known uses of pulsars for testing the predictions of gravitational theories are those in which the predicted strong-field effects are compared directly against observations. As essentially point-like objects in strong gravitational fields, neutron stars in binary systems provide extraordinarily clean tests of these predictions.

In any given theory of gravity, the post-Keplerian (PK) parameters can be written as functions of the pulsar and companion star masses and the Keplerian parameters. As the two stellar masses are the only unknowns in the description of the orbit, it follows that measurement of any two PK parameters will yield the two masses, and that measurement of three or more PK parameters will over-determine the problem and allow for self-consistency checks. It is this test for internal consistency among the PK parameters that forms the basis of the classic tests

of strong-field gravity. It should be noted that the basic Keplerian orbital parameters are well-measured and can effectively be treated as constants here.

In general relativity, the equations describing the PK parameters in terms of the stellar masses are (see [27–29]):

$$\dot{\omega} = 3 \left(\frac{P_b}{2\pi} \right)^{-5/3} (T_\odot M)^{2/3} (1 - e^2)^{-1}, \quad (26)$$

$$\gamma = e \left(\frac{P_b}{2\pi} \right)^{1/3} T_\odot^{2/3} M^{-4/3} m_2 (m_1 + 2m_2), \quad (27)$$

$$\dot{P}_b = -\frac{192\pi}{5} \left(\frac{P_b}{2\pi} \right)^{-5/3} \left(1 + \frac{73}{24}e^2 + \frac{37}{96}e^4 \right) (1 - e^2)^{-7/2} T_\odot^{5/3} m_1 m_2 M^{-1/3}, \quad (28)$$

$$r = T_\odot m_2, \quad (29)$$

$$s = x \left(\frac{P_b}{2\pi} \right)^{-2/3} T_\odot^{-1/3} M^{2/3} m_2^{-1}. \quad (30)$$

where $s \equiv \sin i$, $M = m_1 + m_2$ and $T_\odot \equiv GM_\odot/c^3 = 4.925490947 \mu\text{s}$. Other theories of gravity, such as those with one or more scalar parameters in addition to a tensor component, will have somewhat different mass dependencies for these parameters.

A traditional method of comparing the observed results to the predictions of GR is through use of a “mass-mass” diagram. As an example, a recent mass-mass diagram for PSR B1534+12 shown in Figure 1. This presents the 68% confidence regions for parameters measured using the theory-independent “DD” formalism, which makes no assumptions about the validity of any gravitational theory. If these curves intersect in a common region which includes the mass predictions based on GR, then the parameters may be said to agree with GR. (Note that the two neutron-star masses are then also well determined, up to an unmeasurable Doppler-shift correction [27].) These plots were pioneered for the original DNS (indeed the original binary pulsar) PSR B1913+16 [87, 88]. That 7.75-hour-orbit system, which brought its discoverers Hulse and Taylor the 1993 Nobel Prize in Physics, shows an excellent agreement with GR based on the measured PK parameters $\dot{\omega}$, γ and \dot{P}_b [89]. The slightly less eccentric system PSR B1534+12 allows detection of Shapiro delay in addition to the $\dot{\omega}$, \dot{P}_b and γ parameters measured for B1913+16, permitting an $\dot{\omega}$ - γ - s combination which tests only the quasi-static regime of GR, an important complement to the “mixed” B1913+16 test [90]. The offset of \dot{P}_b for B1534+12 from its expected GR value can be attributed to a poorly known necessary kinematic correction due to the relative acceleration of the pulsar-system center-of-mass and Solar System Barycenter reference frames [91]. The crucial unknown quantity is the distance to the pulsar. Under the assumption that GR is correct, the distance can be derived to be $1.04 \pm 0.04 \text{ kpc}$ [7].

The recently-discovered double pulsar system PSR J0737–3039 [8, 9, 92] is of course of especial interest. In addition to the five PK parameters measurable as for PSR B1534+12, the existence of two radio pulsars in the system allows a measurement of the mass ratio $R = a_1/a_2 = m_2/m_1$, where a_1 and a_2 are the semi-major axes of the two orbits. This parameter places an entirely new and unique line on the mass-mass diagram for the system (e.g., [92]) and is moreover the same function of the two masses in all theories of gravity, independent of self-gravitational effects. Indeed, the combination of R and $\dot{\omega}$ can be used to predict s very precisely in the context of GR, and the measured value agrees with this prediction to within 0.22% [92]. This system offers exciting potential for the future as well: because of its 2.4-hour orbit, the strong-field effects are the largest known. The parameter $\dot{\omega}$ will soon be measured to such precision as to make it likely that higher-order post-Newtonian expansion terms will be needed to describe it. In particular, it may be possible to measure the contribution from the spin-orbit coupling of the recycled “A” pulsar, which would lead directly to a measurement of the moment of inertia of A and hence a tremendously important constraint on neutron-star equations of state [92, 93].

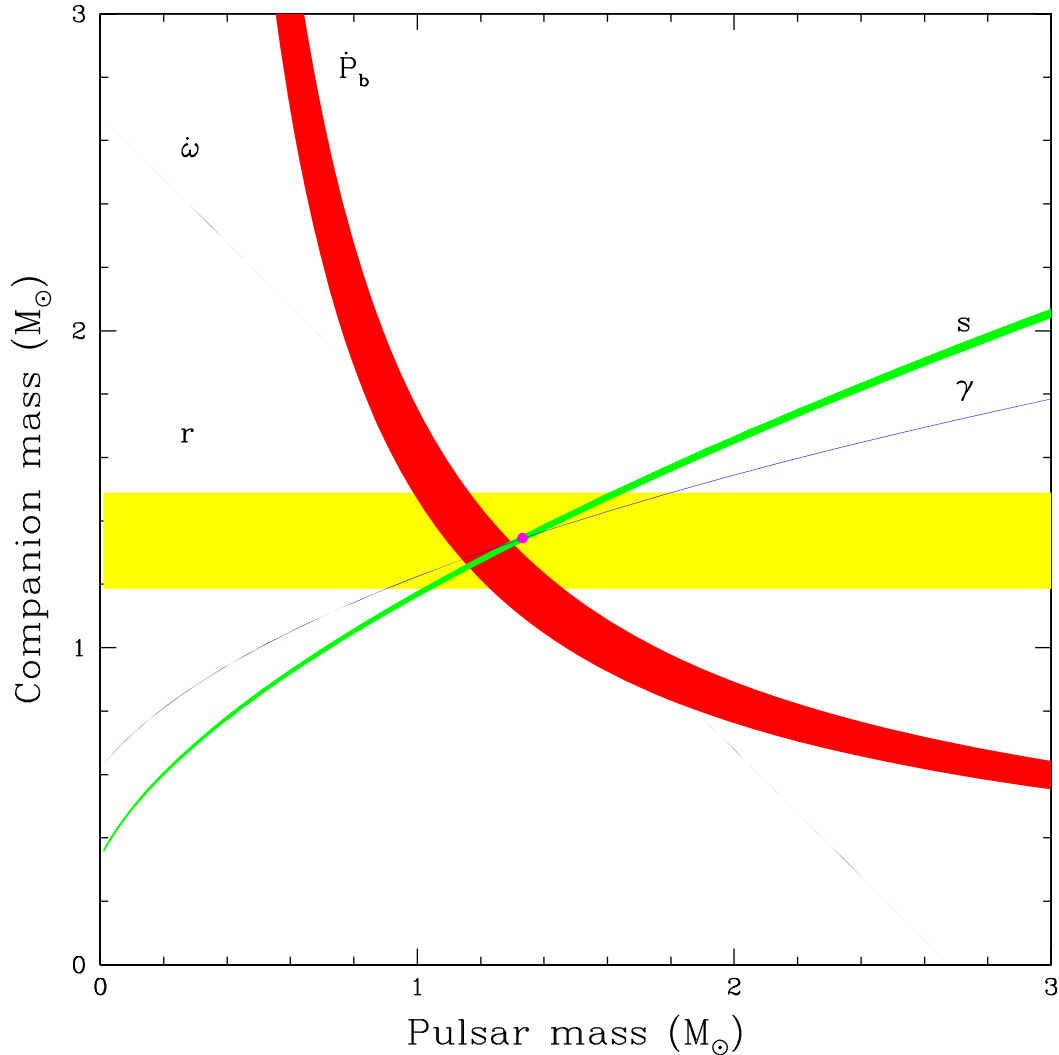


Figure 1: Mass-mass diagram for the PSR B1534+12 system. Labeled curves illustrate 68% confidence ranges of the DD parameters (Stairs et al., unpublished). The filled circle indicates the component masses according to the general-relativistic solution. The kinematic correction for assumed distance $d = 0.7 \pm 0.2$ kpc has been subtracted from the observed value of \dot{P}_b ; the uncertainty on this kinematic correction dominates the uncertainty of this curve. A slightly larger distance removes the small apparent discrepancy between the observed and predicted values of this parameter.

The circular-orbit PSR–WD system J0437–4715 has a fully known orientation due to geometrical effects and the motions of the pulsar and the Earth [43, 94, 95]. The magnitude and shape of the Shapiro delay signal can be predicted based on the geometrically derived system inclination and compared to the predictions of GR; this results in an excellent match [43]. The same argument could be made for the wider-orbit PSR J1713+0747 for which the same angles have recently been measured [44].

There are several other recently discovered highly relativistic systems. The eccentric young-pulsar–white-dwarf system PSR J1141–6545 [62] permits measurement of $\dot{\omega}$, \dot{P}_b and γ through timing [63, 64] and $\sin i$ through scintillation [96]; all these parameters are in good agreement with GR. A near twin of the Hulse-Taylor pulsar was found in the Parkes Multibeam survey [97] but does not yet have a long enough timing baseline to provide a test of GR. Another relativistic system with a young pulsar, PSR J1906+0746 [98], was among the first discoveries of the Arecibo

L-band Feed Array (ALFA) pulsar survey [99]; it is not yet known whether its companion is a white dwarf or a second neutron star. All of these systems promise to put independent constraints on deviations from GR. It will also be fruitful to combine the measurements from all systems to produce global constraints on theories (e.g., [66, 100]).

4.1. Spin-Orbit Coupling and Geodetic Precession

The evolutionary scenarios for double-NS systems (e.g., [101, 102]) predict that, immediately before the second supernova explosion, the two stellar spin axes should be aligned with the orbital angular momentum of the system. After the explosion, the recycled pulsar’s spin axis direction should be unchanged, but the orbital angular momentum vector and most likely the spin axis of the companion will have changed direction. The resulting misalignment between the recycled pulsar’s spin axis and the orbital angular momentum vector (expected to be roughly 20° [103]) will cause both vectors will precess about the total angular momentum of the system. In practice, the total angular momentum is completely dominated by the orbital angular momentum. The evolution of the pulsar spin axis \mathbf{S}_1 can be written as [4, 5]:

$$\frac{d\mathbf{S}_1}{dt} = \boldsymbol{\Omega}_1^{\text{spin}} \times \mathbf{S}_1, \quad (31)$$

where the vector $\boldsymbol{\Omega}_1^{\text{spin}}$ is aligned with the orbital angular momentum. Its magnitude is given by:

$$\Omega_1^{\text{spin}} = \frac{1}{2} \left(\frac{P_b}{2\pi} \right)^{-5/3} \frac{m_2(4m_1 + 3m_2)}{(1 - e^2)(m_1 + m_2)^{4/3}} T_\odot^{2/3}, \quad (32)$$

where again $T_\odot \equiv GM_\odot/c^3 = 4.925490947 \mu\text{s}$. The predicted precession periods are roughly 700 years for PSR B1534+12, 300 years for PSR B1913+16, 270 years for PSR J1141–6545 and only 70–75 years for PSRs J0737–3039A and B. The primary manifestation of this precession is expected to be a slow change in the shape of the pulse profile, as different regions of the pulse emission beam move into the observable slice.

Profile shape changes have been known in the Hulse-Taylor binary for 20 years [104], with a clear change in the relative heights of the two profile peaks over several years. While the obvious interpretation of these changes was taken to be geodetic precession, a quantitative test of the precession rate was impossible because the intrinsic pulse beam shape was unknown. Thus the major use of the geodetic precession in this system has in fact been in beam modeling. Interestingly, although a simple picture of a cone-shaped beam might lead to an expectation of a change in the *separation* of the peaks with time, no evidence for this was seen until the late 1990s, at the Effelsberg 100-m telescope [105], by which point the two peaks had begun to move closer together at a rather fast rate. This changing peak separation, along with the predicted precession rate and a simple conal model of the pulse beam, yields a spin-orbit misalignment angle of about 22° and a prediction that the pulsar will disappear from view in about 2025 [105], in good agreement with an earlier prediction [106] made before the peak separation began to change. Recent results from Arecibo [107] confirm the gist of these results, with a misalignment angle of about 21° , but preferring an hourglass-shaped beam. If the rate of precession is allowed to vary as another free parameter in the pulse-shape fit, a value of $1.2^\circ \pm 0.2^\circ$ is derived [108, 109]. This is consistent with the GR prediction but still depends on the beam-shape model and is therefore not a true test of the precession rate.

The situation is different for PSR B1534+12, which has stronger signal-to-noise in general and which has a polarization position angle swing that follows the rotating vector model [111]. In fact, for this pulsar, long-term changes are apparent in *both* the profile shape and in the polarization properties. The polarization changes show that the impact parameter of the line of sight to the pulsar’s magnetic pole is increasing in magnitude at a rate of about $0.2^\circ/\text{yr}$ (Figure 2). Under the assumption that this is due to geodetic precession of the spin axis, these changes provide an immediate insight into the 3-dimensional orientation of the pulsar’s spin axis. Furthermore, the long-term evolution of the pulse profile shape can be modeled linearly and compared in magnitude changes to smaller but similar variations due to special-relativistic aberration on orbital timescales. Thus the unknown intrinsic pulse beam shape can be “calibrated out” and the precession rate measured [112]. While the rate measurement is still low-precision,

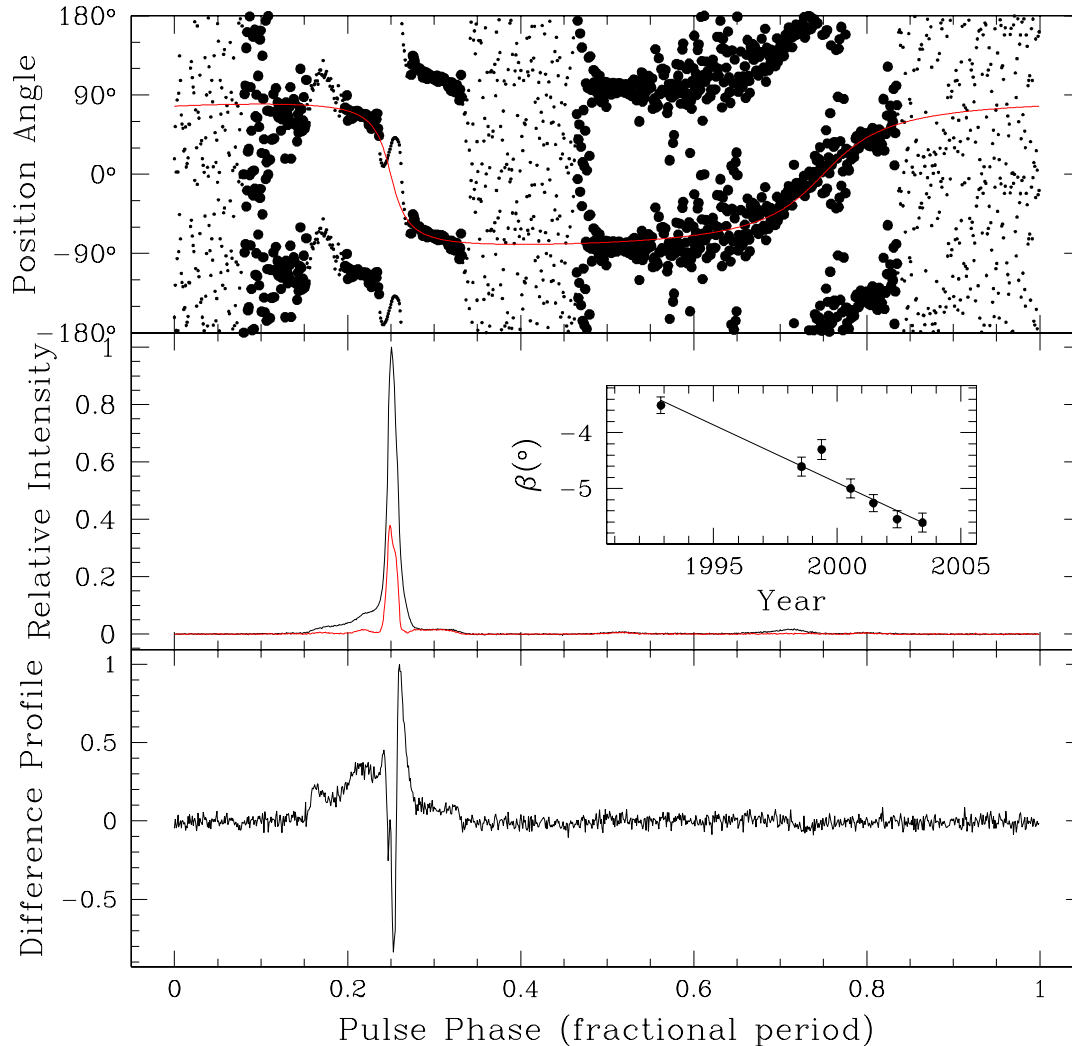


Figure 2: Top panel: the position angle of linear polarization in 2001 June, with best fit rotating vector model (RVM) overlaid in red. Middle panel: total intensity (black) and linear polarization (red) profiles in 2001 June. This profile is very similar in shape to the “reference” profile. Inset: evolution of impact angle β with time. Bottom panel: “Difference” profile, representing essentially the time-derivative of the observed profile. Adapted from [110]

it is in excellent agreement with the predictions of GR. Besides providing the first beam-model-independent test of the precession rate in strong-field gravity, these observations also yield the full 3-dimensional system geometry for B1534+12 and permit stringent constraints on the mass of the progenitor to the second NS as well as the asymmetric kick during the second supernova explosion [113, 114].

Geodetic precession has also been observed in the pulsar–white-dwarf system PSR J1141–6545 [116] and there is some evidence for the effect in the newly discovered PSR J1906+0746 [98]. Intriguingly, profile shape changes have been seen in only the younger of the J0737–3039 pulsars [117, 118].

5. Conclusions

The next several years will be very exciting times for pulsar tests of GR, with better timing leading to superior equivalence-principle violation limits, potential for improving the precession rate test in PSR B1534+12 using wider-bandwidth observations, and the prospect of qualitatively new as well as unprecedentedly precise tests resulting from the double-pulsar system.

In the longer term, large-scale pulsar surveys, such as those now underway at Arecibo [99] or focusing on globular clusters (e.g., [86]), are likely to yield exciting new relativistic or exotic systems, potentially including the “holy grail” of a pulsar–black-hole binary. Such a system (if these in fact exist in reasonable numbers) is quite likely to be found by the Square Kilometre Array, which will be sensitive to pulsars clear through our Galaxy and into neighboring galaxies such as M31 [115]. The next decade or two promise to be exciting times for pulsar searchers and for those looking to set ever-more-stringent limits on deviations from General Relativity.

Acknowledgments

The author holds an NSERC UFA and is supported by a Discovery Grant. She thanks Michael Kramer for a careful reading of the manuscript.

References

- [1] R. A. Hulse, J. H. Taylor, *ApJ* **201**, L55 (1975).
- [2] R. V. Wagoner, *ApJ* **196**, L63 (1975).
- [3] D. M. Eardley, *ApJ* **196**, L59 (1975).
- [4] T. Damour, R. Ruffini, *Comptes Rendus, Serie A – Sciences Mathematiques* **279**, 971 (1974).
- [5] B. M. Barker, R. F. O’Connell, *Phys. Rev. D* **12**, 329 (1975).
- [6] I. H. Stairs, *Living Reviews in Relativity* **6**, 5 (2003).
- [7] I. H. Stairs, Rasio and Stairs [119], pp. 3–18.
- [8] M. Burgay, *et al.*, *Nature* **426**, 531 (2003).
- [9] A. G. Lyne, *et al.*, *Science* **303**, 1153 (2004).
- [10] A. Hewish, S. J. Bell, J. D. H. Pilkington, P. F. Scott, R. A. Collins, *Nature* **217**, 709 (1968).
- [11] F. Pacini, *Nature* **219**, 145 (1968).
- [12] T. Gold, *Nature* **218**, 731 (1968).
- [13] D. C. Backer, S. R. Kulkarni, C. Heiles, M. M. Davis, W. M. Goss, *Nature* **300**, 615 (1982).
- [14] E. S. Phinney, S. R. Kulkarni, *ARAA* **32**, 591 (1994).
- [15] T. M. Tauris, E. P. J. van den Heuvel, *ArXiv Astrophysics e-prints* (2003).
- [16] O. Maron, J. Kijak, M. Kramer, R. Wielebinski, *A&AS* **147**, 195 (2000).
- [17] T. H. Hankins, B. J. Rickett, *Methods in Computational Physics Volume 14 – Radio Astronomy* (Academic Press, New York, 1975), pp. 55–129.
- [18] D. C. Backer, *et al.*, *PASP* **109**, 61 (1997).
- [19] F. A. Jenet, W. R. Cook, T. A. Prince, S. C. Unwin, *PASP* **109**, 707 (1997).
- [20] I. H. Stairs, E. M. Splaver, S. E. Thorsett, D. J. Nice, J. H. Taylor, *MNRAS* **314**, 459 (2000).
- [21] J. H. Taylor, *Philos. Trans. Roy. Soc. London A* **341**, 117 (1992).
- [22] A. W. Hotan, M. Bailes, S. M. Ord, *MNRAS* **362**, 1267 (2005).
- [23] E. M. Standish, *A&A* **114**, 297 (1982).
- [24] E. M. Standish, *JPL Planetary and Lunar Ephemerides, DE405/LE405, Memo IOM 312.F-98-048* (JPL, Pasadena, 1998). [Http://ssd.jpl.nasa.gov/iau-comm4/de405iom/de405iom.pdf](http://ssd.jpl.nasa.gov/iau-comm4/de405iom/de405iom.pdf).
- [25] D. C. Backer, R. W. Hellings, *ARAA* **24**, 537 (1986).

- [26] T. Damour, N. Deruelle **43**, 107 (1985).
- [27] T. Damour, N. Deruelle, *Ann. Inst. H. Poincaré (Physique Théorique)* **44**, 263 (1986).
- [28] J. H. Taylor, J. M. Weisberg, *ApJ* **345**, 434 (1989).
- [29] T. Damour, J. H. Taylor, *Phys. Rev. D* **45**, 1840 (1992).
- [30] C. W. Misner, K. S. Thorne, J. A. Wheeler, *Gravitation* (W. H. Freeman, San Francisco, 1973).
- [31] C. M. Will, *Theory and Experiment in Gravitational Physics* (Cambridge University Press, Cambridge, 1993).
- [32] C. M. Will, K. J. Nordtvedt, *ApJ* **177**, 757 (1972).
- [33] C. Will, *Living Reviews in Relativity* **4**, 4 (2001).
- [34] T. Damour, G. Esposito-Farèse, *Class. Quant Grav.* **9**, 2093 (1992).
- [35] T. Damour, G. Esposito-Farèse, *Phys. Rev. D* **53**, 5541 (1996).
- [36] C. M. Will, *ApJ* **393**, L59 (1992).
- [37] M. Konacki, A. Wolszczan, I. H. Stairs, *ApJ* **589**, 495 (2003).
- [38] K. Nordtvedt, *Phys. Rev.* **170**, 1186 (1968).
- [39] J. O. Dickey, *et al.*, *Science* **265**, 482 (1994).
- [40] T. Damour, G. Schäfer, *Phys. Rev. Lett.* **66**, 2549 (1991).
- [41] N. Wex, *A&A* **317**, 976 (1997).
- [42] K. Kuijken, G. Gilmore, *MNRAS* **239**, 571 (1989).
- [43] W. van Straten, *et al.*, *Nature* **412**, 158 (2001).
- [44] E. M. Splaver, D. J. Nice, I. H. Stairs, A. N. Lommen, D. C. Backer, *ApJ* **620**, 405 (2005).
- [45] N. Wex, *Pulsar Astronomy - 2000 and Beyond, IAU Colloquium 177*, M. Kramer, N. Wex, R. Wielebinski, eds. (Astronomical Society of the Pacific, San Francisco, 2000), pp. 113–116.
- [46] I. H. Stairs, *et al.*, *ApJ* **632**, 1060 (2005).
- [47] T. Damour, G. Esposito-Farèse, *Phys. Rev. D* **46**, 4128 (1992).
- [48] J. F. Bell, F. Camilo, T. Damour, *ApJ* **464**, 857 (1996).
- [49] F. Camilo, D. J. Nice, J. H. Taylor, *ApJ* **412**, L37 (1993).
- [50] F. Camilo, D. J. Nice, J. H. Taylor, *ApJ* **461**, 812 (1996).
- [51] C. Lange, *et al.*, *MNRAS* **326**, 274 (2001).
- [52] P. J. Callanan, P. M. Garnavich, D. Koester, *MNRAS* **298**, 207 (1998).
- [53] K. Nordtvedt, C. M. Will, *ApJ* **177**, 775 (1972).
- [54] J. F. Bell, *ApJ* **462**, 287 (1996).
- [55] I. S. Shklovskii, *Sov. Astron.* **13**, 562 (1970).
- [56] J. H. Taylor, J. M. Cordes, *ApJ* **411**, 674 (1993).
- [57] J. M. Cordes, T. J. W. Lazio (2002). astro-ph/0207156.
- [58] J. F. Bell, T. Damour, *Class. Quant Grav.* **13**, 3121 (1996).
- [59] T. Damour, G. Esposito-Farèse, *Phys. Rev. D* **54**, 1474 (1996).
- [60] C. Brans, R. H. Dicke, *Phys. Rev.* **124**, 925 (1961).
- [61] D. J. Nice, *et al.*, *ApJ* **634**, 1242 (2005).
- [62] V. M. Kaspi, *et al.*, *ApJ* **543**, 321 (2000).
- [63] M. Bailes, S. M. Ord, H. S. Knight, A. W. Hotan, *ApJ* **595**, L49 (2003).
- [64] M. Bailes, Rasio and Stairs [119], pp. 33–36.
- [65] J.-M. Gérard, Y. Wiaux, *Phys. Rev. D* **66**, 1 (2002).
- [66] G. Esposito-Farèse (2004). Contribution to 10th Marcel Grossmann meeting, gr-qc/0402007.
- [67] C. M. Will, *ApJ* **214**, 826 (1977).
- [68] C. M. Will, H. W. Zaglauer, *ApJ* **346**, 366 (1989).
- [69] N. Rosen, *Gen. Relativ. Gravit.* **4**, 435 (1973).
- [70] W. Ni, *Phys. Rev. D* **7**, 2880 (1973).
- [71] A. Lightman, D. Lee, *Phys. Rev. D* **8**, 3293 (1973).
- [72] J. Weisberg, J. Taylor, *Gen. Relativ. Gravit.* **13**, 1 (1981).

- [73] C. C. Counselman, I. I. Shapiro, *Science* **162**, 352 (1968).
- [74] I. Goldman, *MNRAS* **244**, 184 (1990).
- [75] D. J. Nice, J. H. Taylor, A. S. Fruchter, *ApJ* **402**, L49 (1993).
- [76] D. J. Nice, J. H. Taylor, *ApJ* **441**, 429 (1995).
- [77] Z. Arzoumanian, Radio observations of binary pulsars: Clues to binary evolution and tests of general relativity, Ph.D. thesis, Princeton University (1995).
- [78] R. D. Reasenberg, *Philos. Trans. Roy. Soc. London A* **310**, 227 (1983).
- [79] R. W. Hellings, *et al.*, *Phys. Rev. Lett.* **51**, 1609 (1983).
- [80] M. Toscano, *et al.*, *MNRAS* **307**, 925 (1999).
- [81] T. Damour, G. W. Gibbons, J. H. Taylor, *Phys. Rev. Lett.* **61**, 1151 (1988).
- [82] K. Nordtvedt, *Phys. Rev. Lett.* **65**, 953 (1990).
- [83] J. G. Williams, S. G. Turyshev, D. H. Boggs, *Phys. Rev. Lett.* **93**, 261101 (2004).
- [84] S. Chandrasekhar, *ApJ* **74**, 81 (1931).
- [85] K. S. Thorne, *Compact Stars in Binaries: IAU Symposium 165*, J. van Paradijs, E. P. J. van del Heuvel, E. Kuulkers, eds. (Kluwer, Dordrecht, 1996), pp. 153–183.
- [86] S. M. Ransom, *et al.*, *Science* **307**, 892 (2005).
- [87] R. A. Hulse, J. H. Taylor, *ApJ* **195**, L51 (1975).
- [88] J. H. Taylor, J. M. Weisberg, *ApJ* **253**, 908 (1982).
- [89] J. M. Weisberg, J. H. Taylor, Rasio and Stairs [119], pp. 25–31.
- [90] I. H. Stairs, S. E. Thorsett, J. H. Taylor, A. Wolszczan, *ApJ* **581**, 501 (2002).
- [91] T. Damour, J. H. Taylor, *ApJ* **366**, 501 (1991).
- [92] M. Kramer, *et al.*, *Proc. of the 22nd Texas Symposium on Relativistic Astrophysics* (2005). Astro-ph/0503386.
- [93] J. M. Lattimer, B. F. Schutz, *ApJ* **629**, 979 (2005).
- [94] S. M. Kopeikin, *ApJ* **439**, L5 (1995).
- [95] S. M. Kopeikin, *ApJ* **467**, L93 (1996).
- [96] S. M. Ord, M. Bailes, W. van Straten, *ApJ* **574**, L75 (2002).
- [97] A. J. Faulkner, *et al.*, *ApJ* **618**, L119 (2005).
- [98] D. R. Lorimer, *et al.*, *ApJ* **640**, 428 (2006).
- [99] J. M. Cordes, *et al.*, *ApJ* **637**, 446 (2006).
- [100] J. H. Taylor, A. Wolszczan, T. Damour, J. M. Weisberg, *Nature* **355**, 132 (1992).
- [101] J. D. M. Dewi, O. R. Pols, *MNRAS* **344**, 629 (2003).
- [102] H. A. Bethe, G. E. Brown, *ApJ* **506**, 780 (1998).
- [103] M. Bailes, *A&A* **202**, 109 (1988).
- [104] J. M. Weisberg, R. W. Romani, J. H. Taylor, *ApJ* **347**, 1030 (1989).
- [105] M. Kramer, *ApJ* **509**, 856 (1998).
- [106] Y. N. Istomin, *Sov. Astron. Lett.* **17**, 301 (1991).
- [107] J. M. Weisberg, J. H. Taylor, *ApJ* **576**, 942 (2002).
- [108] M. Kramer, *IX Marcel Grossmann Meeting*, R. J. V.G. Gurzadyan, R. Ruffini, eds. (World Scientific, 2002).
- [109] M. Kramer, O. Löhmer, A. Karastergiou, *Radio Pulsars*, M. Bailes, D. J. Nice, S. Thorsett, eds. (Astronomical Society of the Pacific, San Francisco, 2003), pp. 99–102.
- [110] E. M. Standish, *A&A* **417**, 1165 (2004).
- [111] V. Radhakrishnan, D. J. Cooke, *Astrophys. Lett.* **3**, 225 (1969).
- [112] I. H. Stairs, S. E. Thorsett, Z. Arzoumanian, *Phys. Rev. Lett.* **93**, 141101 (2004).
- [113] S. E. Thorsett, R. J. Dewey, I. H. Stairs, *ApJ* **619**, 1036 (2005).
- [114] B. Willems, V. Kalogera, M. Henninger, *ApJ* **616**, 414 (2004).
- [115] M. Kramer, D. C. Backer, T. J. W. Lazio, B. W. Stappers, S. Johnston **48**, 993 (2004).
- [116] A. W. Hotan, M. Bailes, S. M. Ord, *ApJ* **624**, 906 (2005).
- [117] M. Burgay, *et al.*, *ApJ* **624**, L113 (2005).

[118] R. N. Manchester, *et al.*, *ApJ* **621**, L49 (2005).

[119] F. Rasio, I. H. Stairs, eds., *Binary Radio Pulsars* (Astronomical Society of the Pacific, San Francisco, 2005).